



Thermodynamic Evaluation of the Fe-Zn Binary System with Reference to the Latest Experimental Phase Diagram

Ikuo Ohnuma¹ · Kwangsik Han¹ · Inho Lee¹ · Takako Yamashita² · Ryosuke Kainuma³

Submitted: 31 October 2023 / in revised form: 26 March 2024 / Accepted: 9 April 2024 / Published online: 5 May 2024
© ASM International 2024

Abstract The phase diagram of the Fe-Zn binary system was evaluated based on the CALPHAD method with reference to the latest experimental data. The solubility ranges of the intermetallic compound phases, Γ -Fe₄Zn₉, Γ_1 -Fe₁₁Zn₄₀, δ_{1k} -FeZn₇, δ_{1p} -Fe₁₃Zn₁₂₆, and ζ -FeZn₁₃ were modeled considering their structures consisting of Zn₁₂ icosahedra with Fe at the center (Fe₁Zn₁₂ clusters) as well as glue-like Fe and Zn atoms, and the miscibility gap between the δ_{1k} and δ_{1p} phases was also taken into account in the present calculations. The solubility of Fe in the liquid and (η Zn) phases that was confirmed as dozens of times larger than the values reported in the earlier literature could be calculated by introducing Fe₁Zn₁₂ associates to these solution phases. Consequently, all phase equilibria were adequately reproduced by the thermodynamic models and parameters revised in the present study.

Keywords associate solution model · CALPHAD · intermetallic compound · phase diagram · steel · thermodynamic assessment

1 Introduction

Because of their importance for the high anticorrosive coating formed by hot-dip galvanizing (GI) or galvannealing (GA),^[1] phase equilibria in the Zn-Fe binary system have been studied repeatedly for several decades.^[2–15] A great deal of effort has also been devoted to measuring the thermodynamic properties of the equilibrium phases in the Fe-Zn system over the whole composition range from low to high temperatures.^[16–22] Thanks to these valuable experimental data, the phase diagram of the Fe-Zn binary system was assessed by Burton and Perrot,^[23] which has been accepted as the most reliable experimental phase diagram, and much progress has also been made in attempting phase diagram calculations. Several authors have assessed the phase diagram thermodynamically in the early days of CALPHAD,^[24–26] however, the intermetallic compound (IMC) phases were defined as line compounds, and the magnetic contribution to the Gibbs energy was not taken into account explicitly in those early studies. The experimental phase diagram assessed by Burton and Perrot^[23] was first adequately reproduced by thermodynamic calculations reported by Su et al.,^[27] and the revised evaluation proposed by Nakano et al.,^[28,29] in which the thermodynamic description of the IMC phases was examined using sublattice models based on their crystallographic characteristics. The latter appears to have been adopted in a commercial thermodynamic database of steel materials. After that, some shortcomings in these

This invited article is part of a special tribute issue of the *Journal of Phase Equilibria and Diffusion* dedicated to the memory of Thaddeus B. “Ted” Massalski. The issue was organized by David E. Laughlin, Carnegie Mellon University; John H. Perepezko, University of Wisconsin–Madison; Wei Xiong, University of Pittsburgh; and *JPED* Editor-in-Chief Ursula Kattner, National Institute of Standards and Technology (NIST).

✉ Ikuo Ohnuma
OHNUMA.Ikuo@nims.go.jp

¹ Research Center for Structural Materials, National Institute for Materials Science (NIMS), Tsukuba 305-0047, Japan

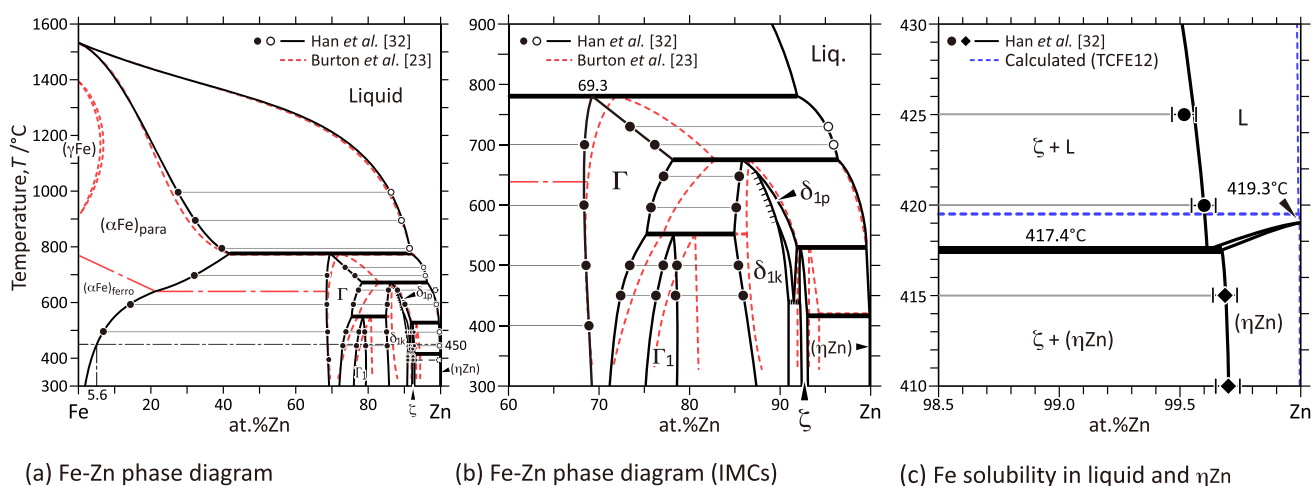
² Materials Integration Research Department, Steel Research Lab., JFE Steel Co., Chiba 260-0835, Japan

³ Department of Materials Science, Graduate School of Engineering, Tohoku University, Sendai 980-8579, Japan

Table 1 Comparison between thermodynamic parameters of the liquid phase^[28–31]

	Nakano ^[28,29]	Xiong ^[30]	Tang ^[31]	Present work
${}^0L_{\text{Fe,Zn}}^{\text{Liq.}}$	+ 58088 − 23.665· <i>T</i>	+ 20696.5073	+ 125613.74 × exp(− 1.38979·10 ^{−3} · <i>T</i>)	+ 20116.2
${}^1L_{\text{Fe,Zn}}^{\text{Liq.}}$	+ 92219 − 55.584· <i>T</i>	+ 14782.0192 − 8.9768· <i>T</i>	+ 189615.062 × exp(− 2.3496·10 ^{−3} · <i>T</i>)	− 150.285
${}^2L_{\text{Fe,Zn}}^{\text{Liq.}}$	+ 13570	− 11266.6992 + 7.3942· <i>T</i>	− 2137.539	− 1561.94
$G_{\text{FeZn}_{12}}$				− 112799.9 + 141.485· <i>T</i>
Notes *	MG at HT appears	MG at HT was corrected	MG at HT was corrected using exponential parameters	Associate solution model was utilized

* “MG” and “HT” in notes represent “miscibility gap” and “high temperature”, respectively.

**Fig. 1** Phase diagrams of the Fe-Zn binary system experimentally determined by Han *et al.*^[32]

evaluations were pointed out by Xiong *et al.*^[30] For instance, an inverse miscibility gap appears in the liquid phase with a minimum-temperature critical point at 1529 °C, which is caused by the negatively large temperature dependence of the composition dependent interaction parameter (${}^1L_{\text{Fe,Zn}}^{\text{Liq.}}$) shown in Table 1. Xiong *et al.* introduced a small negative temperature dependence in ${}^1L_{\text{Fe,Zn}}^{\text{Liq.}}$ ^[30] and Tang *et al.* introduced an exponential temperature dependence in ${}^0L_{\text{Fe,Zn}}^{\text{Liq.}}$ and ${}^1L_{\text{Fe,Zn}}^{\text{Liq.}}$ ^[31] as listed in Table 1, thereby resolving the problem of the inverse miscibility gap.

In our previous study, we determined the phase equilibria involving the IMC phases in the Fe-Zn binary system at temperatures from 400 to 1000 °C by the alloying method described in Ref. [32]. In the latest phase diagram shown in Fig. 1,^[32] five IMC phases, Γ , Γ_1 , δ_{1k} , δ_{1p} , and ζ , exist stably as equilibrium phases, in which the δ_{1k} and δ_{1p} phases were considered as a single phase of δ_1 in both experimental^[23] and calculated^[27–31] phase diagrams.

Since significant differences in the formation behavior^[33] and mechanical properties^[34] are recognized between the δ_{1k} and δ_{1p} phases, the phase equilibria, including the miscibility gap¹ associated with these two phases, need to be properly evaluated by thermodynamic calculations. Furthermore, the solubility ranges of IMC phases in the Zn-rich portion mostly shift toward the Fe-rich direction^[32,35] in comparison with the phase diagram in the literature as shown in Fig. 1. It is also noteworthy that the Fe solubility in the liquid Zn, for instance 0.5 at.% at 450 °C, was revised to be 17 times as large as the generally assessed value in the literature, 0.03 at.%. Therefore, there remains the potential for improving the thermodynamic evaluation

¹ A “miscibility gap” is a type of two-phase equilibrium between isostructural phases that share a single Gibbs energy curve with an upward convexity due to positive interaction, magnetic transition, order-disorder transition, *etc.*, and a second order phase transformation may occur between them at higher temperatures. In the present study, however, the Gibbs energies of the disordered δ_{1p} and the ordered δ_{1k} phases were evaluated separately.

Table 2 Nominal symbols, stoichiometric ratios, crystal structures, and formula of Gibbs energy models in Zn-Fe binary system

Phase	Pearson symbol	Space group	Prototype	Formula in the present study
Liquid	(Fe, Zn, FeZn ₁₂)
(αFe)	<i>cI2</i>	<i>Im</i> $\bar{3}m$	W	(Fe, Zn) ₁ (Va) ₃
(γFe)	<i>cF4</i>	<i>Fm</i> $\bar{3}m$	Cu	(Fe, Zn) ₁ (Va) ₁
Γ-Fe ₄ Zn ₉	<i>cI52</i>	<i>I</i> $\bar{4}3m$	Cu ₅ Zn ₈	(Fe) _{0.0667} ^I (Zn) _{0.6} ^{II} (Fe, Zn) _{0.3333} ^{III}
Γ ₁ -Fe ₁₁ Zn ₄₀	<i>cF408</i>	<i>F</i> $\bar{4}3m$	Fe ₁₁ Zn ₄₀	(Fe) _{0.0769} ^I (Zn) _{0.6923} ^{II} (Fe, Zn) _{0.2308} ^{III}
δ _{1k} -FeZn ₇	Three times as large as that of δ _{1p}			(Fe) _{0.0714} ^I (Zn) _{0.7143} ^{II} (Fe, Zn) _{0.2143} ^{III}
δ _{1p} -Fe ₁₃ Zn ₁₂₆	<i>hP555</i>	<i>P6</i> ₃ <i>mc</i>	FeZn ₁₀	(Fe) _{0.0714} ^I (Zn) _{0.7143} ^{II} (Fe, Zn) _{0.2143} ^{III}
ζ-FeZn ₁₃	<i>mC28</i>	<i>C2/m</i>	CoZn ₁₃	(Fe) _{0.0667} ^I (Zn) _{0.7333} ^{II} (Fe, Zn) _{0.2} ^{III}
(ηZn)	<i>hP2</i>	<i>P6</i> ₃ / <i>mmc</i>	Mg	(Fe, Zn, FeZn ₁₂) ₁ (Va) _{0.5}

of the Fe-Zn binary phase diagram. To improve the accuracy of the thermodynamic calculation based on the latest experimental data, the crystal structures as well as the solubility composition ranges of the five IMC phases need to be considered. Recently, Inui et al. suggested that all the IMC phases in the Fe-Zn system have a principle for constructing their crystal structures,^[36] which can be understood by considering the packing of coordinated polyhedra with the common structural unit being the Zn₁₂ and/or (Zn, Fe)₁₂ icosahedron whose central site is exclusively occupied by an Fe atom. They also suggested that with increasing Fe content in the IMC phases the geometry linking the Fe-centered icosahedra changes from vertex-sharing to face-sharing, Zn atoms on the face-sharing sites are partially substituted by Fe atoms, and the fraction of isolated Zn atoms decreases. These crystallographic characteristics need to be considered for a thermodynamic model of the IMC phases. Furthermore, the strong tendency for the crystal structures of all IMC phases to consist of icosahedral Fe₁Zn₁₂ clusters suggests that Fe₁Zn₁₂ clusters may coexist with Fe and Zn solute atoms in the Zn-rich liquid phase and ηZn (hcp) phase. In view of the above situation, the associate solution model considering Fe₁Zn₁₂ clusters was adopted for the Gibbs energy description of the Zn-rich liquid and ηZn (hcp) phases.

Therefore, we carried out a thermodynamic evaluation of the Fe-Zn binary system in this study to solve the above issues remaining from previous thermodynamic evaluations^[27–31] by applying the associate solution model for the Gibbs energy description of the liquid and ηZn (hcp) phases.

2 Thermodynamic Description

2.1 Gibbs Energy of Solution Phases

The molar Gibbs energy of the αFe (bcc) and γFe (fcc) solution phases were described by sub-regular solution approximation,

$$G_m^\phi = G_{Fe}^\phi \cdot x_{Fe} + G_{Zn}^\phi \cdot x_{Zn} + RT\{x_{Fe}\ln(x_{Fe}) + x_{Zn}\ln(x_{Zn})\} + x_{Fe}x_{Zn} \cdot L_{Fe,Zn}^\phi, \tag{Eq 1}$$

where G_{Fe}^ϕ and G_{Zn}^ϕ represent the Gibbs energies of pure Fe and pure Zn, respectively, in the corresponding structure of ϕ . x_{Fe} and x_{Zn} are the mole fractions of Fe and Zn, respectively. $L_{Fe,Zn}^\phi$ represents the interaction parameter, which has a composition dependence in the form of the Redlich-Kister (RK) polynomial^[37] described by the following equation:

$$L_{Fe,Zn}^\phi = \sum_n (x_{Fe} - x_{Zn})^n \cdot {}^nL_{Fe,Zn}^\phi. \tag{Eq 2}$$

In addition to the Gibbs energy described by Eq 1, the magnetic contribution to the Gibbs energy, G_{mag}^ϕ , which was originally proposed by Inden^[38,39] and simplified by Hillert and Jarl,^[40] is appended for the αFe bcc (A2) and γFe fcc (A1) phases.

On the other hand, the Gibbs energies of the liquid (L) and ηZn (hcp) phases were described by the associate solution model,^[41,42]

$$G^\psi = y_{Fe}G_{Fe}^\psi + y_{Zn}G_{Zn}^\psi + y_{Fe_1Zn_{12}}G_{Fe_1Zn_{12}}^\psi + RT\{y_{Fe}\ln(y_{Fe}) + y_{Zn}\ln(y_{Zn}) + y_{Fe_1Zn_{12}}\ln(y_{Fe_1Zn_{12}})\} + y_{Fe}y_{Zn}L_{Fe,Zn}^\psi + y_{Fe}y_{Fe_1Zn_{12}}L_{Fe,Fe_1Zn_{12}}^\psi + y_{Zn}y_{Fe_1Zn_{12}}L_{Zn,Fe_1Zn_{12}}^\psi, \tag{Eq 3}$$

where considerable amount of Fe₁Zn₁₂ associates is assumed to co-exist with Fe and Zn atoms in these Zn-rich solution phases as mentioned in Introduction. G_i^ψ , y_i , and $L_{i,j}^\psi$ represent the Gibbs energy of each component i ($i = Fe, Zn$ and Fe₁Zn₁₂ associate), the site fraction of i , and the interaction parameter between components i and j , respectively. $L_{i,j}^\psi$ also has a composition dependence in the form of the Redlich-Kister (RK) polynomial^[37] in the same

Table 3 Thermodynamic and magnetic parameters of the Fe-Zn system evaluated in this study

Thermodynamic parameters, J/mol and magnetic parameters, K, μ_B
Liquid : (Fe, Zn, FeZn ₁₂)
${}^0L_{\text{Fe,Zn}}^L = + 20116.2, {}^1L_{\text{Fe,Zn}}^L = - 150.285, {}^2L_{\text{Fe,Ni}}^L = - 1561.94$
$L_{\text{Fe,Fe}_1\text{Zn}_{12}}^L = L_{\text{Zn,Fe}_1\text{Zn}_{12}}^L = 0$
$G_{\text{Fe}_1\text{Zn}_{12}}^L = - 8676.917 + 10.8835 \text{ T} + 0.0769 G_{\text{Fe}}^L + 0.9231 G_{\text{Zn}}^L$
$\alpha\text{Fe (A2)} : (\text{Fe, Zn})_1 (\text{Va})_3$
${}^0L_{\text{Fe,Zn}}^{A2} = - 8169.109 + 16.6657 \text{ T}, {}^1L_{\text{Fe,Zn}}^{A2} = + 13656.92 - 13.9237 \text{ T},$
${}^2L_{\text{Fe,Zn}}^{A2} = + 4485.963$
$T_C^{A2} = 1043x_{\text{Fe}} + 504.3x_{\text{Fe}}x_{\text{Zn}}, \beta^{A2} = 2.22x_{\text{Fe}}$
$\gamma\text{Fe (A1)} : (\text{Fe, Zn})_1 (\text{Va})_1$
${}^0L_{\text{Fe,Zn}}^{A1} = + 12487.70, {}^1L_{\text{Fe,Zn}}^{A1} = + 1441.752$
$T_C^{A1} = -201x_{\text{Fe}}, \beta^{A1} = -2.1x_{\text{Fe}}$
$\eta\text{Zn (A3)} : (\text{Fe, Zn, FeZn}_{12})_1 (\text{Va})_{0.5}$
${}^0L_{\text{Fe,Zn}}^{A3} = + 1500 + 5 \text{ T}, L_{\text{Fe,Fe}_1\text{Zn}_{12}}^{A3} = L_{\text{Zn,Fe}_1\text{Zn}_{12}}^{A3} = 0$
$G_{\text{Fe}_1\text{Zn}_{12}}^{A3} = - 284.615 + 0.0769 G_{\text{Fe}}^{A3} + 0.9231 G_{\text{Zn}}^{A3}$
$\Gamma\text{-Fe}_4\text{Zn}_9 : (\text{Fe})_{0.0667}^I (\text{Zn})_{0.6}^{II} (\text{Fe, Zn})_{0.3333}^{III}$
$G_{\text{Fe:Zn:Fe}}^\Gamma = - 4003.232 + 0.7346 \text{ T} + 0.4 \text{ }^\circ G_{\text{Fe}}^{A2} + 0.6 \text{ }^\circ G_{\text{Zn}}^{A3}$
$G_{\text{Fe:Zn:Zn}}^\Gamma = + 2515.325 - 4.3415 \text{ T} + 0.0667 \text{ }^\circ G_{\text{Fe}}^{A2} + 0.9333 \text{ }^\circ G_{\text{Zn}}^{A3}$
$L_{\text{Fe:Zn:Fe,Zn}}^\Gamma = - 18228.68 + 19.9038 \text{ T}$
$\Gamma_1\text{-Fe}_{11}\text{Zn}_{40} : (\text{Fe})_{0.0769}^I (\text{Zn})_{0.6923}^{II} (\text{Fe, Zn})_{0.2308}^{III}$
$G_{\text{Fe:Zn:Fe}}^{\Gamma_1} = - 5485.973 + 2.5583 \text{ T} + 0.3077 \text{ }^\circ G_{\text{Fe}}^{A2} + 0.6923 \text{ }^\circ G_{\text{Zn}}^{A3}$
$G_{\text{Fe:Zn:Zn}}^{\Gamma_1} = + 4399.436 - 6.3696 \text{ T} + 0.0769 \text{ }^\circ G_{\text{Fe}}^{A2} + 0.9231 \text{ }^\circ G_{\text{Zn}}^{A3}$
$L_{\text{Fe:Zn:Fe,Zn}}^{\Gamma_1} = - 20229.49 + 20.8641 \text{ T}$
$\delta_{1k}\text{-FeZn}_7 : (\text{Fe})_{0.0714}^I (\text{Zn})_{0.7143}^{II} (\text{Fe, Zn})_{0.2143}^{III}$
$G_{\text{Fe:Zn:Fe}}^{\delta_{1k}} = - 6786.998 + 4 \text{ T} + 0.2857 \text{ }^\circ G_{\text{Fe}}^{A2} + 0.7143 \text{ }^\circ G_{\text{Zn}}^{A3}$
$G_{\text{Fe:Zn:Zn}}^{\delta_{1k}} = - 2432.079 - 0.2861 \text{ T} + 0.0714 \text{ }^\circ G_{\text{Fe}}^{A2} + 0.9286 \text{ }^\circ G_{\text{Zn}}^{A3}$
$L_{\text{Fe:Zn:Fe,Zn}}^{\delta_{1k}} = - 1233.705 + 2.4548 \text{ T}$
$\delta_{1p}\text{-Fe}_{13}\text{Zn}_{126} : (\text{Fe})_{0.0714}^I (\text{Zn})_{0.7143}^{II} (\text{Fe, Zn})_{0.2143}^{III}$
$G_{\text{Fe:Zn:Fe}}^{\delta_{1p}} = - 6646.204 + 4 \text{ T} + 0.2857 \text{ }^\circ G_{\text{Fe}}^{A2} + 0.7143 \text{ }^\circ G_{\text{Zn}}^{A3}$
$G_{\text{Fe:Zn:Zn}}^{\delta_{1p}} = - 2088.477 - 0.79 \text{ T} + 0.0714 \text{ }^\circ G_{\text{Fe}}^{A2} + 0.9286 \text{ }^\circ G_{\text{Zn}}^{A3}$
$L_{\text{Fe:Zn:Fe,Zn}}^{\delta_{1p}} = - 1300 + 3 \text{ T}$
$\zeta\text{-FeZn}_{13} : (\text{Fe})_{0.0667}^I (\text{Zn})_{0.7333}^{II} (\text{Fe, Zn})_{0.2}^{III}$
$G_{\text{Fe:Zn:Fe}}^\zeta = + 46222.16 + 3.9874 \text{ T} + 0.2667 \text{ }^\circ G_{\text{Fe}}^{A2} + 0.7333 \text{ }^\circ G_{\text{Zn}}^{A3}$
$G_{\text{Fe:Zn:Zn}}^\zeta = - 2699.545 + 0.1895 \text{ T} + 0.0667 \text{ }^\circ G_{\text{Fe}}^{A2} + 0.9333 \text{ }^\circ G_{\text{Zn}}^{A3}$
$L_{\text{Fe:Zn:Fe,Zn}}^\zeta = - 54547.42$

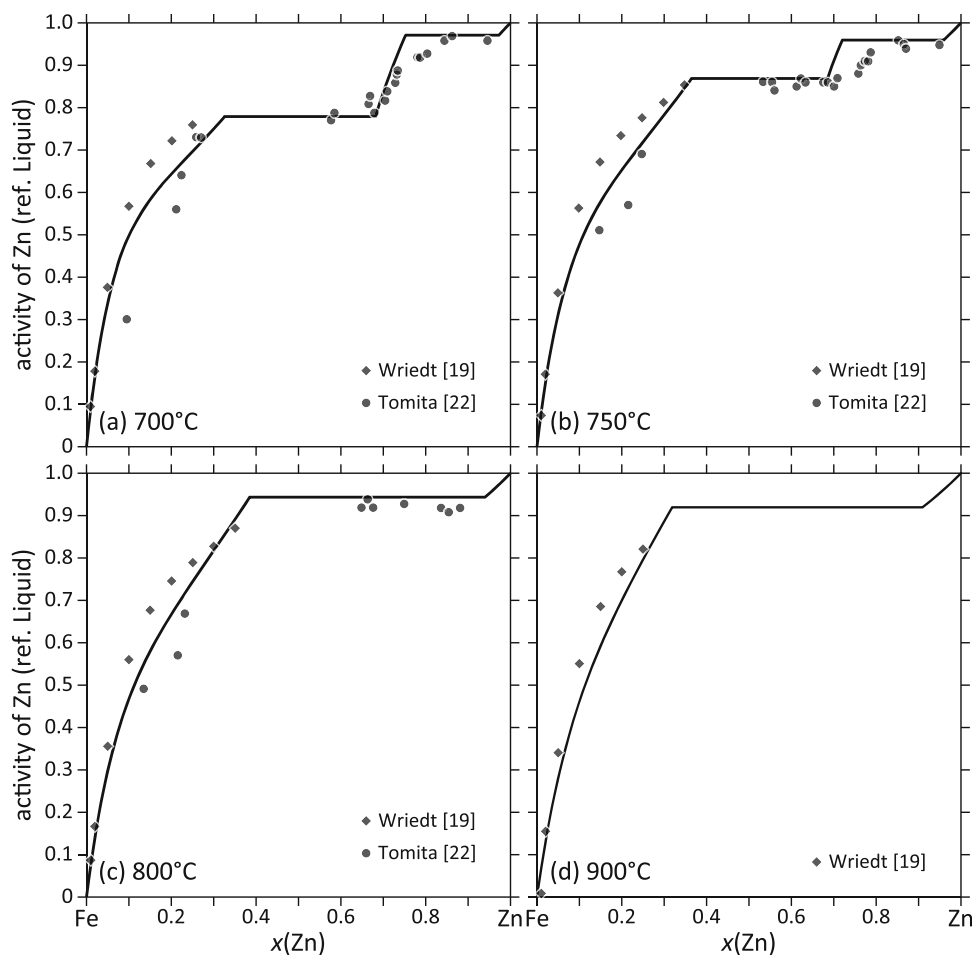
Gibbs energy parameters of pure elements are taken from Ref. [43] and the magnetic properties of disordered solution phases, $\gamma\text{Fe (A1)}$ and $\alpha\text{Fe (A2)}$, are from Ref. [28].

way with Eq 2, however, values both $L_{\text{Fe,Fe}_1\text{Zn}_{12}}^\psi$ and $L_{\text{Zn,Fe}_1\text{Zn}_{12}}^\psi$ were assumed to be zero for simplification. G values for pure elements of Fe and Zn were taken from the SGTE database, [43] whereas $G_{\text{Fe}_1\text{Zn}_{12}}^\psi$ and L values were evaluated based on experimental data from the literature [4,16–22,32] using the PARROT module of Thermo-Calc software. [44]

2.2 Gibbs Energy of Intermetallic Compound Phases

As described in the Introduction, five kinds of IMC phases, ζ , δ_{1k} , δ_{1p} , Γ_1 , and Γ appear stably in the phase diagram of the Fe-Zn system and all IMC phases are basically composed of $\text{Fe}_1\text{Zn}_{12}$ clusters with different linkage geometries and glue-like elements of Fe and Zn. To describe the Gibbs

Fig. 2 Activity of Zn in equilibrated Fe-Zn alloys calculated at temperatures from 700 to 900 °C compared with experimental data^[19,22].



energy of these IMC phases, such complicated crystal structures ideally need to be incorporated into their thermodynamic models. For the practical reasons, however, a three sublattice model, $(\text{Fe})_p^I(\text{Zn})_q^{\text{II}}(\text{Fe}, \text{Zn})_r^{\text{III}}$, for the five IMC phases was applied to describe their Gibbs energy,

$$G_m^\theta = G_{\text{Fe:Zn:Fe}}^\theta \cdot y_{\text{Fe}}^{\text{III}} + G_{\text{Fe:Zn:Zn}}^\theta \cdot y_{\text{Zn}}^{\text{III}} + rRT \{ y_{\text{Fe}}^{\text{III}} \ln(y_{\text{Fe}}^{\text{III}}) + y_{\text{Zn}}^{\text{III}} \ln(y_{\text{Zn}}^{\text{III}}) \} + y_{\text{Fe}}^{\text{III}} y_{\text{Zn}}^{\text{III}} \cdot L_{\text{Fe:Zn:Fe,Zn}}^\theta \quad (\text{Eq 4})$$

Values of p , q , and r ($p + q + r = 1$), where the ratio p/q and the value of r are not exactly but roughly assumed as the Fe/Zn substitution in the $\text{Fe}_7\text{Zn}_{12}$ icosahedra cluster and the fraction of the glue-like site, respectively, were fixed to reproduce the solubility composition range of each IMC phase θ ($\theta = \zeta, \delta_{1k}, \delta_{1p}, \Gamma_1$, or Γ) as listed in Table 2 which also includes the crystal structure information of the stable phases in the Fe-Zn system. $G_{\text{Fe:Zn:Fe}}^\theta$ and $G_{\text{Fe:Zn:Zn}}^\theta$ represent the Gibbs energy of the $\text{Fe}_p\text{Zn}_q\text{Fe}_r$ and $\text{Fe}_p\text{Zn}_q\text{Zn}_r$ compound phases, respectively. $y_{\text{Fe}}^{\text{III}}$ and $y_{\text{Zn}}^{\text{III}}$ represent the site fractions of Fe and Zn, respectively, and $L_{\text{Fe:Zn:Fe,Zn}}^\theta$ is the interaction parameter between Fe and Zn in the third sublattice (III). Temperature dependent functions of $G_{\text{Fe:Zn:Fe}}^\theta$,

$G_{\text{Fe:Zn:Zn}}^\theta$, and $L_{\text{Fe:Zn:Fe,Zn}}^\theta$ with the Eq 2-type composition dependence were evaluated to reproduce experimental data from the literature.^[4,16–22,32] It should be noted that the δ_{1k} and δ_{1p} phases were reported to have an order-disorder (O-DO) relationship with both first- and second-order transformations.^[9,10] In the present study, however, the Gibbs energies of the δ_{1k} and δ_{1p} phases were defined with the same formula of $(\text{Fe})_{0.0714}^I(\text{Zn})_{0.7143}^{\text{II}}(\text{Fe}, \text{Zn})_{0.2143}^{\text{III}}$, but treated as different phases without considering the O-DO relationship for simplicity. Evaluated thermodynamic parameters were summarized in Table 3.

3 Results

3.1 Thermodynamic Properties

The calculated activities of Zn over the entire composition range at 700, 750 and 800 °C, and in the αFe (bcc) phase at 900 °C, where the liquid Zn was chosen as a reference state, are shown in Fig. 2 together with the experimental results reported by Wriedt^[18,19] and Tomita et al.^[22]

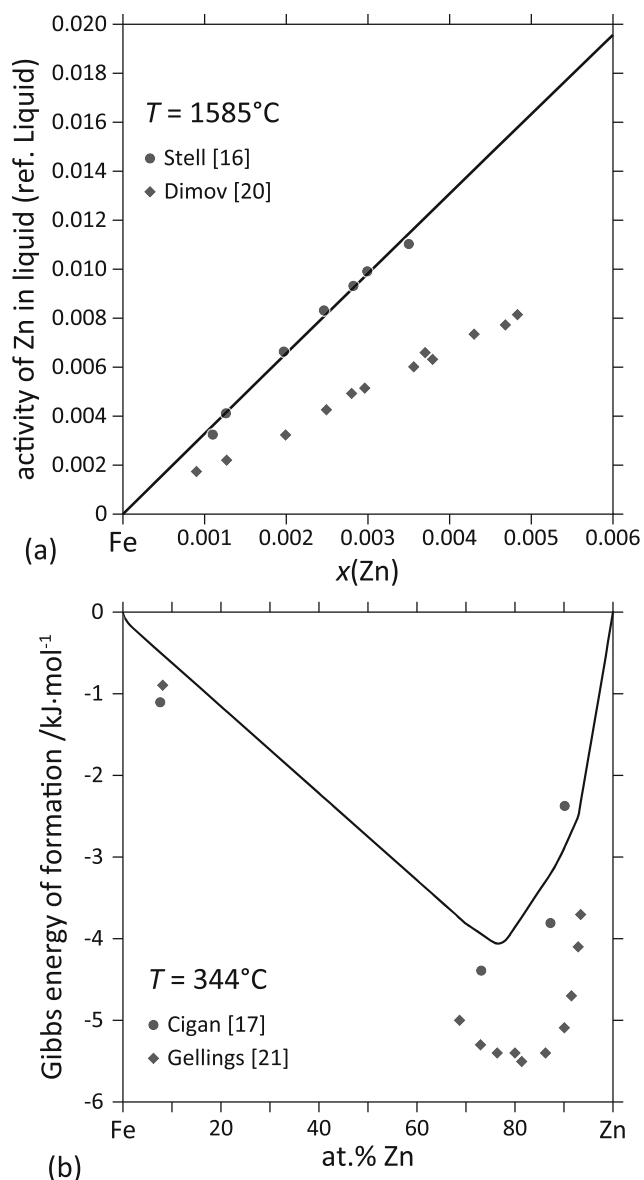


Fig. 3 (a) Comparison of the activity of Zn in Fe-rich liquid alloys calculated at 1585°C with experimental data^[16,20]. (b) Comparison of the formation Gibbs energy of Fe-Zn alloys calculated at 344°C with experimental data^[17,21].

Overall, there is satisfactory agreement between the present calculations and the experimental results. Other examples of comparisons between calculated thermodynamic properties and corresponding experimental data are shown in Fig. 3. Figure 3(a) shows good agreement between the calculated activity of Zn in liquid alloys at 1585°C and its experimental data reported by Stell.^[16] The Gibbs energies of formation of the solid phases at 344°C reported by Cigan^[17] were used rather than those of Gellings et al.^[21] due to the large measurement error of $\pm 2 \text{ kJ mol}^{-1}$ of Gellings et al. as shown in Fig. 3(b).

3.2 Phase Diagrams

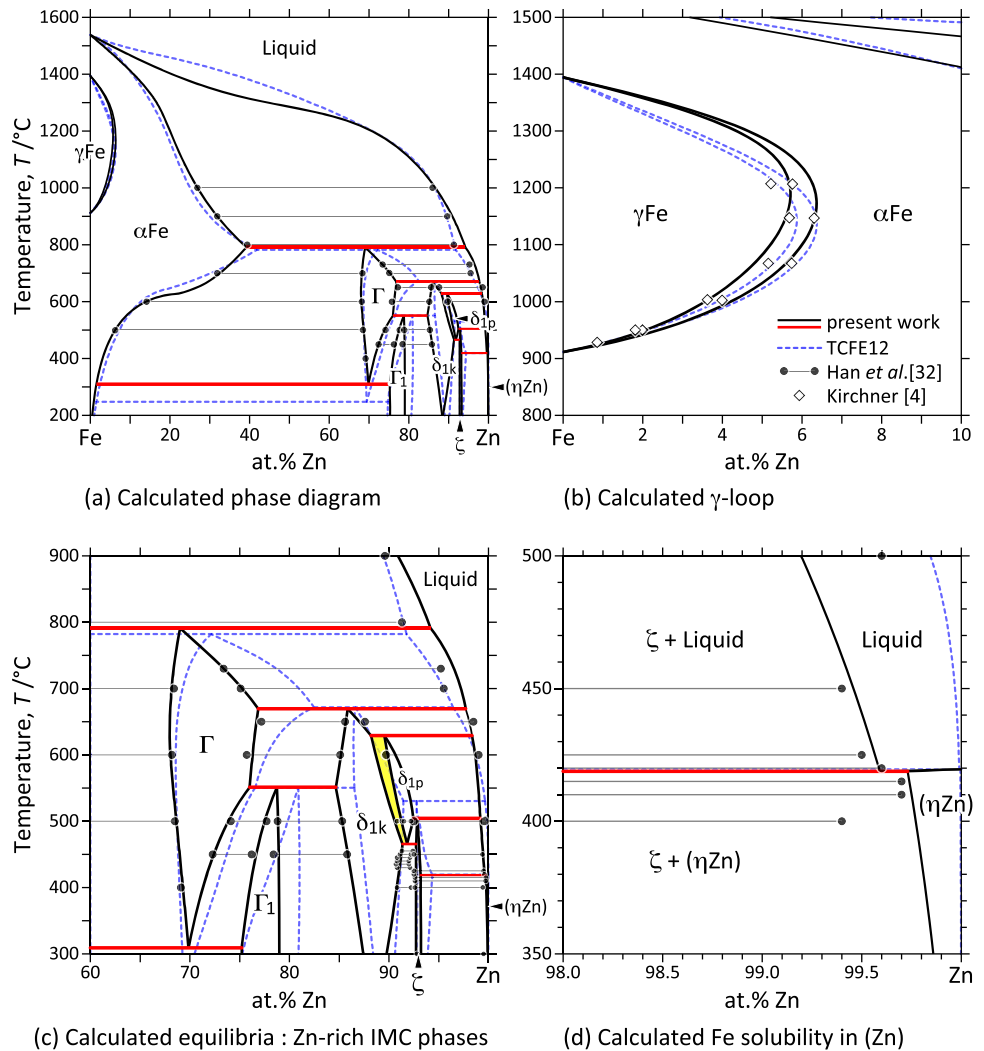
The calculated phase diagram of the Fe-Zn system over the entire composition range is shown in Fig. 4(a), compared with the latest experimental data reported by Han et al.^[32] and the calculated phase diagram using the TCFE12 thermodynamic database.^[45] On the solubility of Zn in the $\alpha\text{Fe}(\text{bcc})$ phase, both of calculated phase boundaries and experimental data are in close agreement, whereas the calculated liquidus curves in the Fe-rich composition side exhibit considerable discrepancy, which cannot be resolved due to lack of experimental data. The focus is on the γ -loop, *i.e.* the phase equilibrium between the $\gamma\text{Fe}(\text{fcc})$ and $\alpha\text{Fe}(\text{bcc})$ phases in Fig. 4(b). The agreement between the present calculations and the experimental data^[4] appears to be better at temperatures in the lower half of the γ -loop than with TCFE12 and worse in the upper half. The phase diagram associated with the five IMC phases of ζ , δ_{1k} , δ_{1p} , Γ_1 , and Γ on the Zn-rich composition side at lower temperatures is shown in Fig. 4(c). As discussed in the Introduction, there were considerable discrepancies between the latest experimental data and the calculations of the phase boundaries using TCFE12, which has been dramatically improved by the present calculations, as shown in Fig. 4(c). Furthermore, the δ_{1k} and δ_{1p} phases, which in previous calculations were regarded as a single phase of δ_1 , were reasonably distinguished in the present assessment. An enlarged phase diagram of the vicinity of the liquid $\rightarrow (\eta\text{Zn}) + \zeta\text{-FeZn}_{13}$ eutectic reaction is shown in Fig. 4(d), where considerable discrepancy is observed between the Fe solubility in the liquid and $\eta\text{Zn}(\text{hcp})$ phases from the latest experimental data and the phase boundaries from previous experiments and calculations. In the present evaluation, the introduction of $\text{Fe}_1\text{Zn}_{12}$ associates in the Gibbs energy model of the liquid and (ηZn) solution phases adequately reproduced the Fe solubility of about 0.3 at.% in the (ηZn) phase and more than 0.4 at.% in the liquid Zn phase, which are almost twenty times as large as the values reported in the literature, as shown in Fig. 4(d).

4 Discussion

4.1 Effect of Associates on the Gibbs Energy of Solution Phases

As discussed above, the crystal structures of all the IMC phases appearing in the phase diagram of the Fe-Zn system are composed of $\text{Fe}_1\text{Zn}_{12}$ clusters with different linkage geometries and glue-like elements of Fe and Zn, which indicates that a significant amount of $\text{Fe}_1\text{Zn}_{12}$ clusters coexists with Fe and Zn solute atoms in the Zn-rich liquid

Fig. 4 Comparison of the phase diagrams of the Fe-Zn binary system calculated in this study with the phase diagrams calculated using the TCFE12 thermodynamic database and experimental data^[4,32]. Calculated miscibility gap between δ_{1k} and δ_{1p} phases is colored yellow in (c). The legend shown in (b) is common to (a) through (d).



and (ηZn) phases, affecting the thermodynamic stability of these Zn-rich phases. In the present calculation, it was quite difficult to reproduce the large Fe solubility in the Zn-rich liquid and (ηZn) phases without introducing the $\text{Fe}_1\text{Zn}_{12}$ associate into the Gibbs energy models of those solution phases. In order to confirm the effect of the $\text{Fe}_1\text{Zn}_{12}$ associate on the Gibbs energy of the liquid phase, the site fraction of $\text{Fe}_1\text{Zn}_{12}$ associates ($y_{\text{Fe}_1\text{Zn}_{12}}$) in the liquid phase under the equilibrium condition was calculated at temperatures from 450 to 800 °C over the entire composition range. Calculated results are shown in Fig. 5. All the $y_{\text{Fe}_1\text{Zn}_{12}}-x_{\text{Zn}}$ curves exhibit a maximum peak and a shoulder, the latter of which corresponds to the chemical composition of the $\text{Fe}_1\text{Zn}_{12}$ associate at $x_{\text{Zn}} = 0.923$. The $y_{\text{Fe}_1\text{Zn}_{12}}$ value of the maximum peak decreases with increasing temperature mainly due to the temperature dependence of the Gibbs energy parameter, $G_{\text{Fe}_1\text{Zn}_{12}}^L$, shown in Table 3. The x_{Zn} value at the maximum peak also decreases with increasing temperature, which may be due

to the effect of increasing entropy at high temperatures. Figure 6 compares the Gibbs energies of Fe-Zn liquid alloys calculated using the associate solution model at temperatures from 450 to 800 °C with those calculated excluding the $\text{Fe}_1\text{Zn}_{12}$ associate. The reference states of Fe and Zn are bcc (A2) and liquid, respectively. The Gibbs energy at low temperatures, for instance at 450 °C shown in Fig. 6(d), decreases significantly over the entire composition range, with a sharp decrease near the stoichiometric composition of $\text{Fe}_1\text{Zn}_{12}$ ($x_{\text{Zn}} = 0.923$), which apparently makes it possible to reproduce the large solubility of Fe in the liquid Zn phase as well as in the hcp ηZn phase reported in the latest experimental phase diagram^[32] as shown in Fig. 7(c). On the other hand, the difference between the Gibbs energies including and excluding the $\text{Fe}_1\text{Zn}_{12}$ associate decreases with increasing temperature, which just corresponds to the change with temperature in the site-fraction of the $\text{Fe}_1\text{Zn}_{12}$ associates shown in Fig. 5.

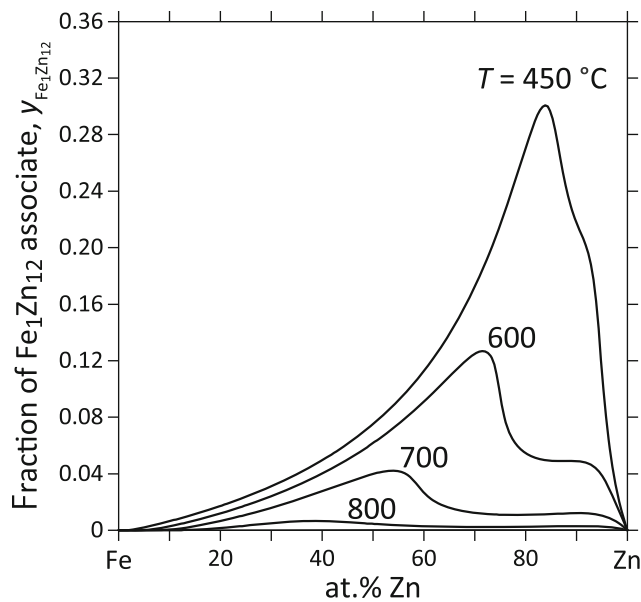


Fig. 5 Site fraction of $\text{Fe}_1\text{Zn}_{12}$ associates in liquid Fe-Zn alloys calculated at temperatures from 450 to 800 °C.

4.2 Effect of Associates on Phase Diagram

Figure 7 compares phase diagram of the Fe-Zn system calculated using the associate solution model with that calculated excluding the $\text{Fe}_1\text{Zn}_{12}$ associate. As shown in Fig. 7(a), differences with and without $\text{Fe}_1\text{Zn}_{12}$ associates are not recognized at temperatures above 800 °C or in the Fe-rich composition range because the $\text{Fe}_1\text{Zn}_{12}$ associate only affects the Gibbs energy of the liquid and (ηZn) phases, and disappears above 800 °C. At temperatures below 800 °C, the stability of the liquid phase is decreased by excluding $\text{Fe}_1\text{Zn}_{12}$ associates, resulting in the decrease of Fe solubility in the liquid phase and in the slight increase of the peritectic temperatures as shown in Fig. 7(b). The effects of the $\text{Fe}_1\text{Zn}_{12}$ associate are observed prominently at the phase boundaries of the Fe solubility in the liquid and (ηZn) phases as shown in Fig. 7(c), which were evaluated using the associate solution model to reproduce the latest experimental data reported by Han et al.^[32]. The exclusion of $\text{Fe}_1\text{Zn}_{12}$ associates from their Gibb energy descriptions reduces the stability of liquid and (ηZn) phases, resulting in a significant decrease in the Fe solubility in these two phases. Interestingly, the associate solution model has made it possible to reproduce the latest experimental data on the solubilities of Fe in the liquid and (ηZn) hcp phases, both of which are about twenty times larger than those reported in the literature. As shown in Table 1, the interaction parameters of the liquid phase (${}^nL_{\text{Fe,Zn}}^{\text{Liq}}$) were revised in the present study without using strong or specific temperature dependences, which indicates that the introduction of $\text{Fe}_1\text{Zn}_{12}$ associates into the liquid and (ηZn) hcp phases

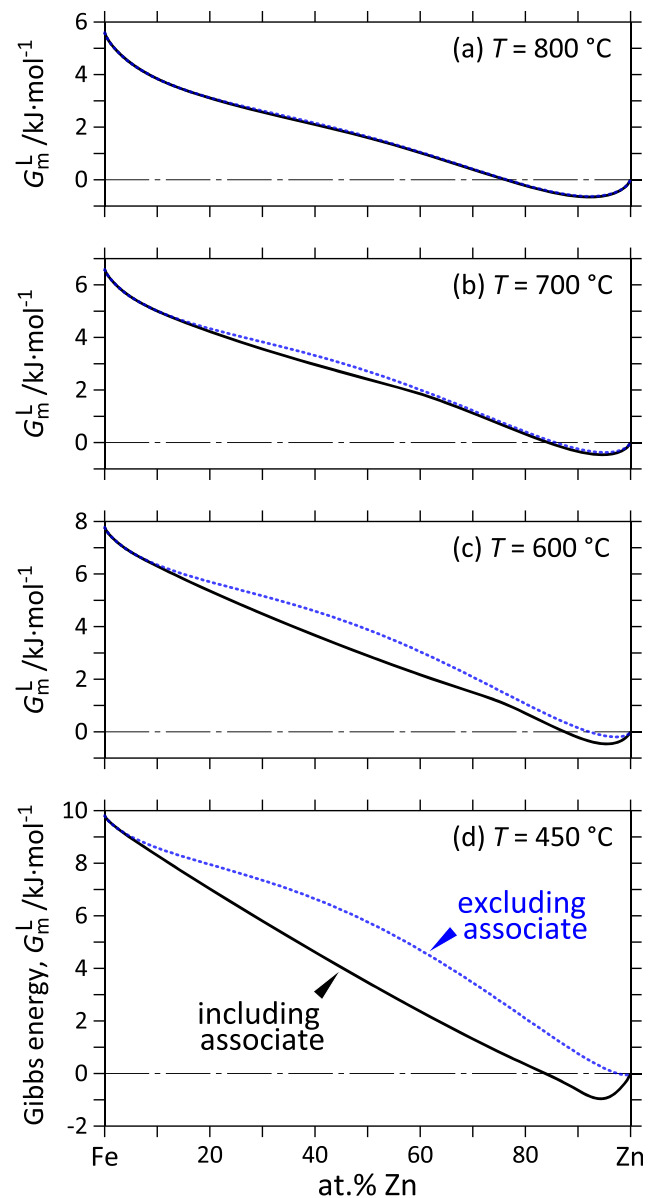


Fig. 6 Gibbs energies of liquid Fe-Zn alloys calculated using the associate solution model at temperatures from 450 to 800 °C compared with those calculated excluding $\text{Fe}_1\text{Zn}_{12}$ associates. Reference states of Fe and Zn are bcc (A2) and liquid, respectively.

appears to be the essence of the atomic state of these phases in the Zn-rich composition range.

Using the consistent set of thermodynamic parameters evaluated in the present study, one can calculate not only the state-of-the-art phase diagram of the Fe-Zn binary system with high accuracy, but also the Gibbs energies of all stable phases in the appropriate solubility range, which can be applicable, for instance, to predict the early stage of the interfacial reaction between an iron sheet and molten Zn.^[33] For the practical application to the hot-dip galvanizing (GI) or galvannealing (GA) processes, it is also expected that the present evaluation could play a

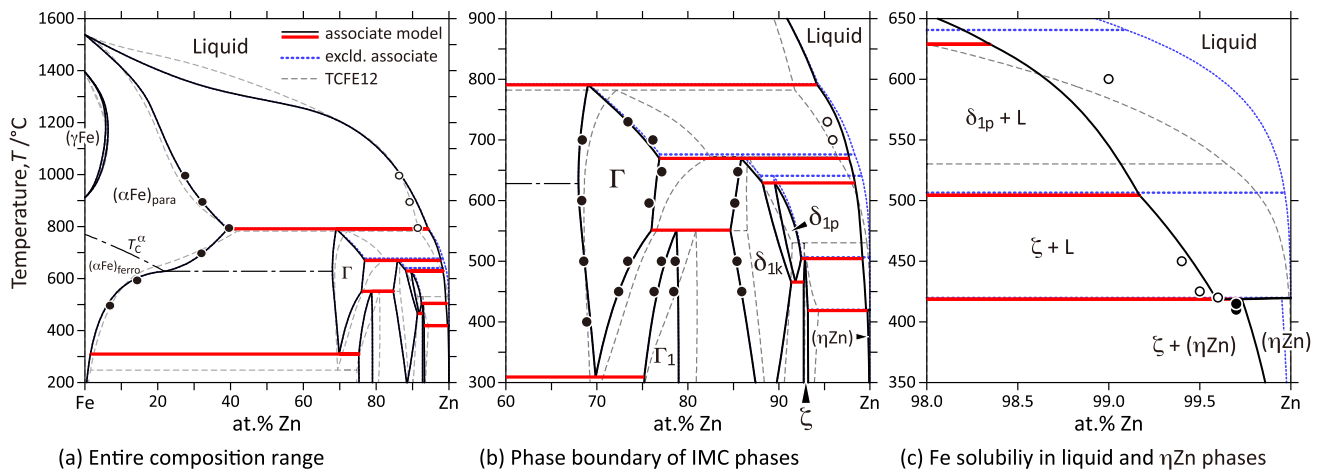


Fig. 7 Comparison of the phase diagrams of the Fe-Zn binary system calculated in this study with the phase diagrams calculated excluding $\text{Fe}_7\text{Zn}_{12}$ associates (denoted by “excl. associate” in (a)) from the Gibbs energy parameters, *i.e.*, $G_{\text{Fe}_7\text{Zn}_{12}}^{\text{L}} = 0$ and $G_{\text{Fe}_7\text{Zn}_{12}}^{\text{A}3} = 0$, in Table 3,

fundamental role for constructing a multi-component thermodynamic database consisting of the elements in steels and molten galvanizing baths.

5 Conclusions

A thermodynamic evaluation of the Fe-Zn binary system was performed using the CALPHAD method over the entire composition range with reference to the latest experimental data. Compared with previous thermodynamic evaluations, the thermodynamic parameters were revised to reproduce the latest and previous experimental data with the following improvements.

- (1) The associate solution model considering $\text{Fe}_7\text{Zn}_{12}$ icosahedron clusters was applied to the Gibbs energy description of the liquid and (ηZn) hcp phases. Consequently, the solubility of Fe in these phases in the latest phase diagram was adequately calculated, and the artificial inverse miscibility gap in the liquid phase at high temperatures was avoided without using strong or specific temperature dependences in the interaction parameters of the liquid phase.
- (2) The three sublattice model of $(\text{Fe})_p^{\text{I}}(\text{Zn})_q^{\text{II}}(\text{Fe}, \text{Zn})_r^{\text{III}}$, considering the crystal structures consisting of Zn_{12} icosahedra with Fe at the center ($\text{Fe}_7\text{Zn}_{12}$ clusters) as well as glue-like Fe and Zn atoms, was applied for the Gibbs energy description of the Γ - Fe_4Zn_9 , Γ_1 - $\text{Fe}_{11}\text{Zn}_{40}$, δ_{1k} - FeZn_7 , δ_{1p} - $\text{Fe}_{13}\text{Zn}_{126}$, and ζ - FeZn_{13} IMC phases. Consequently, the composition ranges of these IMC phases in the latest phase diagram were reproduced well, and the $\delta_{1k} + \delta_{1p}$ miscibility gap was approximately reproduced.

with the phase diagrams calculated using TCFE12 thermodynamic database, and with experimental data (solid and open circles)^[32]. The legend shown in (a) is common to (a) through (c).

- (3) The phase diagrams and thermodynamic properties calculated using the present thermodynamic parameters are in good agreement with the latest phase equilibria and experimental data in the literature, respectively.

Acknowledgments This work was partly supported by the Grants-in-Aid for Scientific Research from JSPS [Grant Number 21H01676].

References

1. A.R. Marder, The metallurgy of zinc-coated steel, *Prog. Mater. Sci.*, 2000, **45**, p 191–271.
2. E.C. Truesdale, R.L. Wilcox, and J.L. Rodda, An investigation of the zinc-rich portion of the system iron-zinc, *Trans. AIME*, 1936, **122**, p 192–230.
3. V.S. Budurov, P. Kovatchev, N. Stojcev, and Z. Kamenova, Über die Eisenseite des Zustandsdiagramms des systems Eisen-Zink, *Z. Metallkd.*, 1972, **63**(6), p 348–350. **in German**
4. G. Kirchner, H. Harvig, K.R. Moquist, and M. Hillert, Die Verteilung von Zink zwischen Ferrit und Austenit und die Thermodynamik des Zweistoffsystems Eisen-Zink, *Arch. Eisenhüttenwes.*, 1973, **44**, p 227–234. **in German**
5. G.F. Bastin, F.J.J. van Loo, and G.D. Rieck, A new compound in the Iron-Zinc system, *Z. Metallkd.*, 1974, **65**(10), p 656–660.
6. G.F. Bastin, F.J.J. van Loo, and G.D. Rieck, On the δ -phase in the Fe-Zn system, *Z. Metallkd.*, 1977, **68**(5), p 359–361.
7. P.J. Gellings, E.W. de Bree, and G. Gierman, Synthesis and characterization of homogeneous intermetallic Fe-Zn compounds. Part I: the δ_1 phase, *Z. Metallkd.*, 1979, **70**(5), p 312–314.
8. P.J. Gellings, G. Gierman, D. Koster, and J. Kuit, Synthesis and characterization of homogeneous intermetallic Fe-Zn compounds. Part III: phase diagram, *Z. Metallkd.*, 1980, **71**(2), p 70–75.
9. R. Kainuma, and K. Ishida, Microstructural evolution of intermetallic compound layers formed in Fe/Zn binary diffusion couples, *Tetsu-to-Hagané*, 2005, **91**(3), p 349–355. **in Japanese**

10. R. Kainuma, and K. Ishida, Reactive diffusion between solid Fe and liquid Zn at 723 K, *ISIJ Int.*, 2007, **47**(5), p 740–744.
11. S. Béllisle, V. Lezon, and M. Gagné, The solubility of Iron in continuous hot-dip galvanizing baths, *J. Phase Equilib.*, 1991, **12**(3), p 259–265.
12. Z.W. Chen, and J.B. See, Dross phases formed in galvanizing baths containing (0-0.1) wt% nickel at 450 °C, *ISIJ Int.*, 1993, **33**(2), p 307–312.
13. N.-Y. Tang, Determination of liquid-phase boundaries in Zn-Fe-Mx systems, *J. Phase Equilib.*, 2000, **21**(1), p 70–77.
14. N.-Y. Tang, and X.B. Yu, Study of the Zinc-rich corner of the Zn-Fe-Cr system at galvanizing temperatures, *J. Phase Equilib. Diffus.*, 2005, **26**(1), p 50–54.
15. J.R. McDermid, M.H. Kaye, and W.T. Thompson, Fe solubility in the Zn-rich corner of the Zn-Al-Fe system for use in continuous galvanizing and galvannealing, *Metall. Mater. Trans. B*, 2007, **38B**, p 215–230.
16. A. Stell, Tablizi dawlenia Parov individualnich westestv, Gos-sudarswenoe izdatelstwo innostranoi literatury, Moskau, 1949.
17. J.M. Cigan, Ph.D. Thesis, Department of Metallurgical Engineering, Carnegie Institute of Technology, July, 1960, pp. 78–87.
18. H.A. Wriedt, and S. Arajs, Ferromagnetic Curie temperatures of some Iron-Zinc solid solutions, *Phys. Status Solidi*, 1966, **16**, p 475–478.
19. H.A. Wriedt, Thermodynamics of ferritic solutions of the iron-zinc system at 700 °C and 900 °C, *Trans. Metall. Soc. AIME*, 1967, **239**, p 1120–1128.
20. I. Dimov, D. Nenov, N. Gidikova, and A. Mozeva, Ermittlung der Zinkaktivität in flüssigen Mangan- und Eisenlegierungen, *Arch. Eisenhüttenwes.*, 1977, **48**, p 209–210. **in German**
21. P.J. Gellings, D. Koster, J. Kuit, and T. Fransen, Synthesis and characterization of homogeneous intermetallic Fe-Zn compounds, Part IV: thermodynamic properties, *Z. Metallkd.*, 1980, **71**(3), p 150–154.
22. M. Tomita, T. Azakami, L.M. Timberg, and J.M. Toguri, The thermodynamics of the Fe-Zn system, *Trans. Jpn. Inst. Met.*, 1981, **22**(10), p 717–722.
23. B.P. Burton and P. Perrot, “Fe–Zn (Iron–Zinc)”, phase diagram of binary iron alloys (monograph series on alloy phase diagrams, vol 9), in ed. by H. Okamoto. ASM Int., 1993, p 459–466.
24. S. Peterson, P.J. Spencer, and K. Hack, A thermodynamic evaluation of the iron-zinc system, *Thermochim. Acta*, 1988, **129**, p 77–87.
25. P. Perrot, and J.Y. Dauphin, Calculation of the Fe-Zn-Si phase diagram between 773 and 1173 K, *CALPHAD Comput. Coupl. Phase Diagr. Thermochem.*, 1988, **12**(1), p 33–40.
26. G. Reumon, P. Perrot, J.M. Fiorani, and J. Hertz, Thermodynamic assessment of the Fe-Zn system, *J. Phase Equilib.*, 2000, **21**(4), p 371–378.
27. X. Su, N.-Y. Tang, and J.M. Toguri, Thermodynamic evaluation of the Fe-Zn system, *J. Alloys Compd.*, 2001, **325**, p 129–136.
28. J. Nakano, D.V. Malakhov, and G.R. Purdy, A crystallographically consistent optimization of the Zn-Fe system, *CALPHAD Comput. Coupl. Phase Diagr. Thermochem.*, 2005, **29**, p 276–288.
29. J. Nakano, D.V. Malakhov, S. Yamaguchic, and G.R. Purdy, A full thermodynamic optimization of the Zn-Fe-Al system within the 420–500 °C temperature range, *CALPHAD Comput. Coupl. Phase Diagr. Thermochem.*, 2007, **31**, p 125–140.
30. W. Xiong, Y. Kong, Y. Du, Z.K. Liu, M. Selleby, and W.H. Sun, Thermodynamic investigation of the galvanizing systems, I: refinement of the thermodynamic description for the Fe–Zn system, *CALPHAD Comput. Coupl. Phase Diagr. Thermochem.*, 2009, **33**, p 433–440.
31. Y. Tang, X. Yuan, Y. Du, and W. Xiong, Thermodynamic modeling of the Fe-Zn system using exponential temperature dependence for the excess Gibbs energy, *J. Min. Metall. Sect. B*, 2011, **47**(1), p 1–10.
32. K. Han, I. Ohnuma, K. Okuda, and R. Kainuma, Experimental determination of phase diagram in the Zn-Fe binary system, *J. Alloys Compd.*, 2018, **737**, p 490–504.
33. K. Han, I. Lee, I. Ohnuma, and R. Kainuma, Formation and growth behavior of intermetallic compound phases in the interfacial reaction of solid Fe/liquid Zn at 450 °C, *J. Alloys Compd.*, 2021, **888**, p 161562.
34. K. Han, I. Lee, I. Ohnuma, K. Okuda, and R. Kainuma, Micro-Vickers hardness of intermetallic compounds in the Zn-rich portion of Zn-Fe binary system, *ISIJ Int.*, 2018, **58**(9), p 1578–1583.
35. L. Zhu, S. Honrao, B. Rijal, R.G. Hennig, and M.V. Manuel, Phase equilibria and diffusion coefficients in the Fe-Zn binary system, *Mater. Des.*, 2020, **188**, p 108437.
36. H. Inui, N.L. Okamoto, and S. Yamaguchi, Crystal structures and mechanical properties of Fe-Zn intermetallic compounds formed in the coating layer of galvannealed steels, *ISIJ Int.*, 2018, **58**(9), p 1550–1561.
37. O. Redlich, and A.T. Kister, Algebraic representation of thermodynamic properties and the classification of solutions, *Ind. Eng. Chem.*, 1948, **40**, p 345–348.
38. G. Inden, In: Proc. Project Meeting CALPHAD V, Düsseldorf, 1976:III.41.
39. G. Inden, The role of magnetism in the calculation of phase diagrams, *Physica B*, 1981, **103**(1), p 82–100.
40. M. Hillert, and M. Jarl, A model for alloying effects in ferromagnetic metals, *CALPHAD Comput. Coupl. Phase Diagr. Thermochem.*, 1978, **2**(3), p 227–238.
41. F. Sommer, Influence of associate formation in alloy-melts on the thermodynamic quantities, *CALPHAD Comput. Coupl. Phase Diagr. Thermochem.*, 1978, **2**(4), p 319–324.
42. N. Saunders, and A.P. Miodownik, *CALPHAD—Calculation of Phase Diagrams, A comprehensive guide* Elsevier, Amsterdam, 1998, p1998
43. A.T. Dinsdale, SGTE data for pure elements, *CALPHAD Comput. Coupl. Phase Diagr. Thermochem.*, 1991, **15**(4), p 317–425.
44. B. Sundman, B. Jansson, and J.-O. Andersson, The Thermo-Calc databank system, *CALPHAD Comput. Coupl. Phase Diagr. Thermochem.*, 1985, **9**(2), p 153–190.
45. “Steel and Fe-Alloys Databases”, Thermo-Calc Software, Stockholm, Sweden (2022). <https://thermocalc.com/products/databases/steel-and-fe-alloys/>

Publisher’s Note Springer Nature remains neutral with regard to jurisdictional claims in published maps and institutional affiliations.

Springer Nature or its licensor (e.g. a society or other partner) holds exclusive rights to this article under a publishing agreement with the author(s) or other rightsholder(s); author self-archiving of the accepted manuscript version of this article is solely governed by the terms of such publishing agreement and applicable law.